Influence of Cr and W Alloying on the Fiber-Matrix Interfacial Shear Strength in Cast and Directionally Solidified Sapphire NiAl Composites

R. ASTHANA, R. TIWARI, and S.N. TEWARI

Sapphire-reinforced NiAl matrix composites with chromium or tungsten as alloying additions were synthesized using casting and zone directional solidification (DS) techniques and characterized by a fiber pushout test as well as by microhardness measurements. The sapphire-NiAl(Cr) specimens exhibited an interlayer of Cr rich eutectic at the fiber-matrix interface and a higher interfacial shear strength compared to unalloyed sapphire-NiAl specimens processed under identical conditions. In contrast, the sapphire-NiAl(W) specimens did not show interfacial excess of tungsten rich phases, although the interfacial shear strength was high and comparable to that of sapphire-NiAl(Cr). The postdebond sliding stress was higher in sapphire-NiAl(Cr) than in sapphire-NiAl(W) due to interface enrichment with chromium particles. The matrix microhardness progressively decreased with increasing distance from the interface in both DS NiAl and NiAl(Cr) specimens. The study highlights the potential of casting and DS techniques to improve the toughness and strength of NiAl by designing dual-phase microstructures in NiAl alloys reinforced with sapphire fibers.

I. INTRODUCTION

IT is now widely recognized that large-scale use of intermetallic β NiAl in high-temperature components is limited due to its low elevated-temperature strength and poor low temperature ductility and toughness in polycrystalline form.[1,2] One potentially attractive technique to overcome some of these problems is reinforcing NiAl with sapphire fibers.[3,4] At present, most sapphire NiAl composites are fabricated using the ''powder cloth'' (PC) or a similar powder metallurgy technique,[4] where the problems associated with binder burnout and polycrystallinity of the matrix tend to impair the toughness as well as the fiber-matrix interfacial shear strength. Recent work has shown[5,6] that cast and directionally solidified (DS) sapphire-NiAl specimens possess interface strength and thermal fatigue resistance superior to PC material. Similar improvements in interface strength in melt-processed composites[7] over hot-pressed composites[8] have been reported in the sapphire-FeAl system.

Liquid metal processing of fiber reinforced intermetallic matrix composites may, therefore, have a distinct advantage over current solid-state fabrication techniques from the standpoint of quality and strength of the interfacial bond. However, casting defects such as matrix and interfacial microvoids may form during liquid state fabrication because of poor wettability, and prevent full realization of fiber strengthening. It is necessary, therefore, to develop techniques to improve the fiber matrix wettability (*e.g.*, by suitable alloying or application of pressure[9]) before the solidification route can be considered viable for making these composites. The reported wetting angles of nickel on sapphire (data are scarce for NiAl) indicate poor wetting.[10] Chromium alloying is known to reduce the contact angle[10] of nickel on sapphire without causing appreciable chemical degradation of sapphire. In addition, the sapphire-nickel bond strength (measured by mechanically pushing the solidified sessile drops off sapphire substrates by application of stress parallel to the substrate) improves significantly through the addition of chromium to nickel.[10,11]

Directional solidification of pseudobinary NiAl-X (where X could be Mo, W, Cr Fe, *etc.*) eutectic alloys has been used previously to create a matrix containing an aligned β phase sandwiched between a ductile second phase. These *in situ* composites of pseudobinary eutectic compositions result in significant improvements in the room-temperature ductility and toughness.[12,13] Directional solidification of NiAl rich (hypoeutectic) compositions could be used to obtain aligned cells of β phase surrounded by the *in situ* composite (DS eutectic) microstructure created by the solidification of the intercellular eutectic liquid. It is likely that these microstructures could also enhance the ductility of NiAl while minimizing the adverse effects of solutes, such as increased alloy density and reduced oxidation resistance, as is the case with solute rich pseudobinary eutectic compositions. Such a matrix structure, when reinforced with sapphire fibers, potentially can improve both the high-temperature strength and the low-temperature ductility and toughness. It is noteworthy that such flexibility in designing matrix microstructure is difficult to achieve by the current solid-state fabrication methods.[4] However, before a detailed characterization of DS proeutectic NiAl alloys reinforced with sapphire fibers can be undertaken, it is necessary to evaluate the influence of solute additions on the interfacial shear strength. Since the fibers are the load bearing constituents at elevated temperatures where NiAl is soft, the strength of the fiber-matrix interfacial bond is of central importance.

R. ASTHANA is a National Research Council Associate with Materials Division, NASA Lewis Research Center, Cleveland, OH 44135. R. TIWARI, formerly Research Associate, Department of Chemical Engineering, Cleveland State University, is with UCAR Carbon Company, Cleveland, OH 44101. S.N. TEWARI, Professor, is with the Department of Chemical Engineering, Cleveland State University, Cleveland, OH 44115.

Manuscript submitted April 4, 1994.

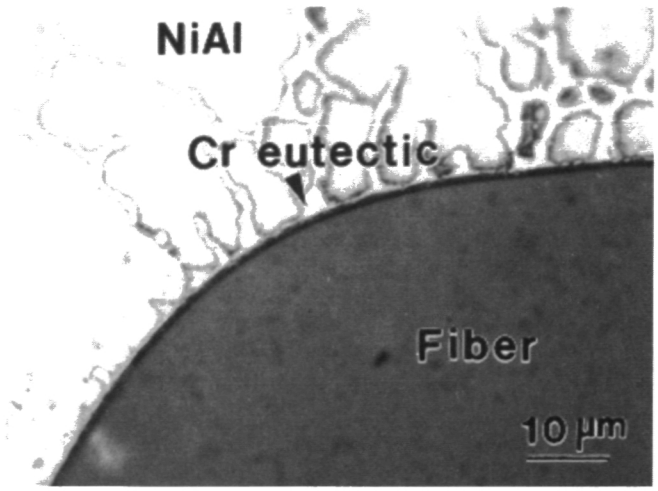

(*a*)

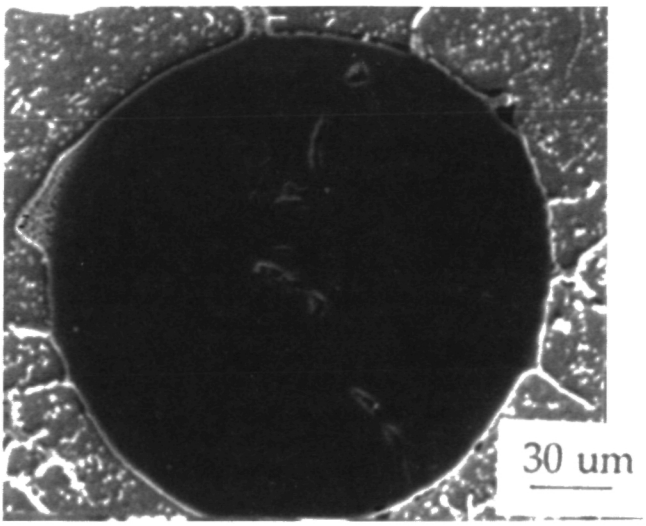

(*b*)

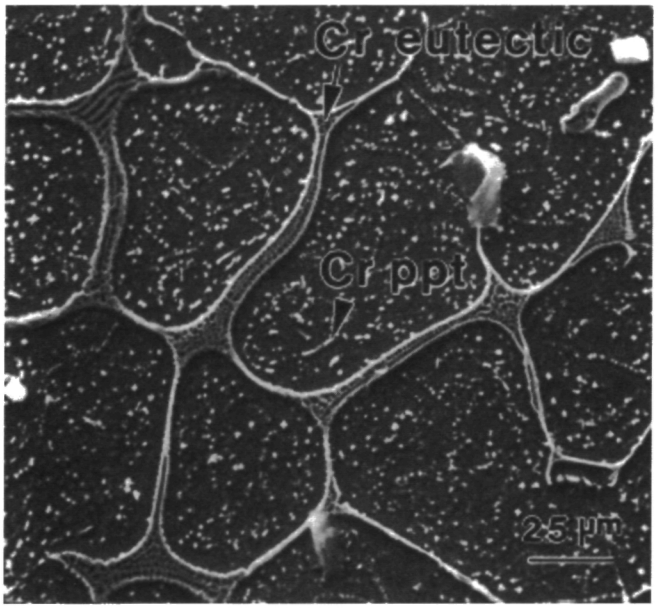

(*c*)

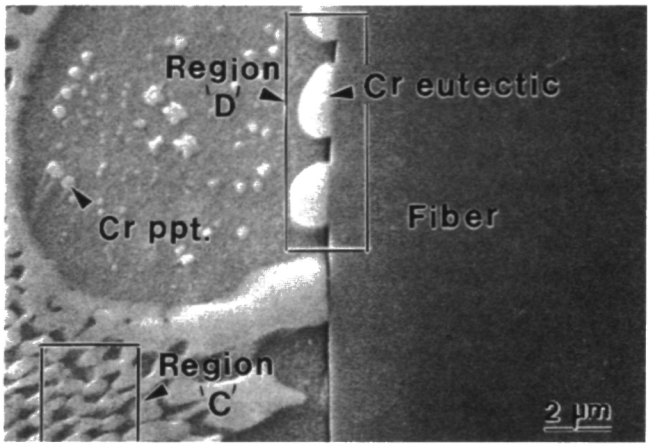

(*d*)

Fig. 1—Fiber-matrix interface in (*a*) AC sapphire-NiAl(Cr); (*b*) fiber-matrix interface in the DS sapphire-NiAl(Cr); (*c*) microstructure of DS NiAl(Cr) showing intercellular Cr eutectic and Cr precipitates within NiAl cells; (*d*) high magnification view of the interface region in the DS sapphire-NiAl(Cr) showing the two types of fiber surroundings (marked C and D) and the excellent bonding between eutectic chromium and sapphire. (*e*) AC sapphire-NiAl(W) and (*f*) DS sapphire-NiAl(W) showing cellular matrix structure and absence of preferential deposition of W-rich phases on sapphire; and (*g*) typical longitudinal view of a DS NiAl(W) specimen showing columnar NiAl grains and cellular microstructure, corresponding to two different growth speeds.

In the present study, proeutectic NiAl(Cr) and NiAl(W) alloys reinforced with sapphire fibers were fabricated using casting and directional solidification techniques and examined for the interfacial shear strength, the thermal cycling (TC) resistance of the composite, and the distribution of matrix microhardness as a function of the distance from the fiber-matrix interface.

II. EXPERIMENTAL PROCEDURE

NiAl, NiAl(Cr), and NiAl(W) alloys were synthesized using vacuum induction melting under a protective, ultrahigh purity argon atmosphere, followed by casting in a high purity copper mold. Alloying of NiAl with chromium and tungsten was performed by arc melting Ni-Cr and Ni-W master alloy pellets that were subsequently diluted with suitable nickel and aluminum charges to obtain the desired chemistry. For composite fabrication, sapphire fibers (single crystal, nominal diameter, 180 μm, supplied by SAPHIKON*, Milford, NH) were laid up in the cavity of a split copper mold using a special fiber layup procedure, followed by gravity pouring and solidification of the molten matrix in the copper mold containing the fibers. The virgin fibers were supplied with sizing that was removed by submersion in deionized water at room temperature for 24 hours. The cast specimens were used as feed material for directional solidification DS in the float zone mode in a 25 kW RF (400 kHz) induction furnace that housed a current concentrator to enhance the coupling

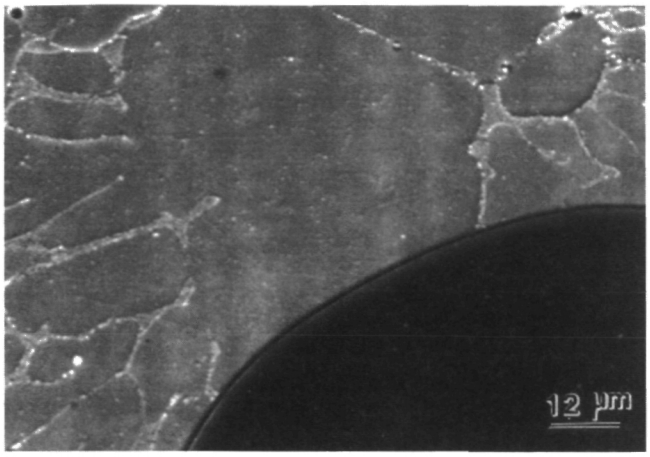

(*e*)

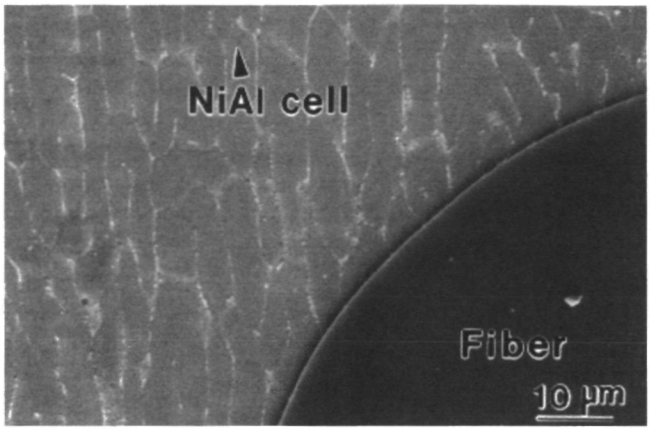

(*f*)

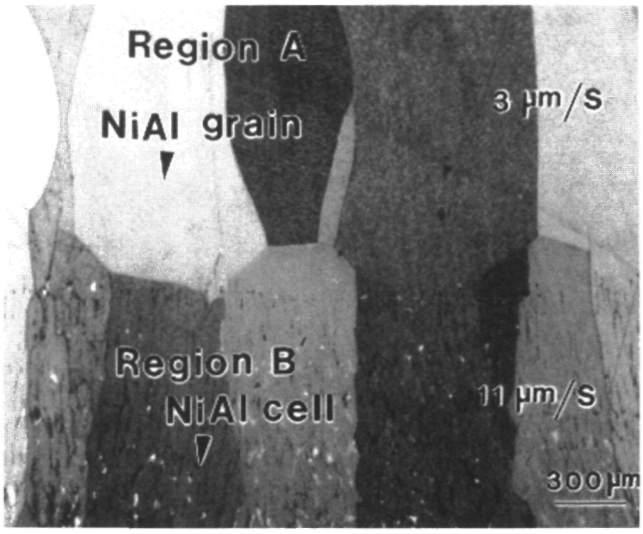

(*g*)

Fig 1.—***(continued):*** Fiber-matrix interface in (*a*) AC sapphire-NiAl(Cr); (*b*) fiber-matrix interface in the DS sapphire-NiAl(Cr); (*c*) microstructure of DS NiAl(Cr) showing intercellular Cr eutectic and Cr precipitates within NiAl cells; (*d*) high magnification view of the interface region in the DS sapphire-NiAl(Cr) showing the two types of fiber surroundings (marked C and D) and the excellent bonding between eutectic chromium and sapphire. (*e*) AC sapphire-NiAl(W) and (*f*) DS sapphire-NiAl(W) showing cellular matrix structure and absence of preferential deposition of W-rich phases on sapphire; and (*g*) typical longitudinal view of a DS NiAl(W) specimen showing columnar NiAl grains and cellular microstructure, corresponding to two different growth speeds.

between the workpiece and the coil, and a motorized traverse mechanism that permitted control of growth speed. Experimental composites with low (<0.5 pct) volume fraction of the fibers were fabricated using this procedure.

The interfacial shear strengths of cast and DS specimens were determined in the ''thin-slice'' configuration using a desktop fiber pushout apparatus[14] that records the load-time (displacement) data during the process of compressing (pushing out) of a single sapphire fiber with the help of a flat bottomed tungsten carbide punch (152 μm diameter). For this purpose, thin discs (200 to 400 μm) with metallographic surface finish were placed over 400 μm wide grooves of a steel sample holder to allow unobstructed pushing of the fibers during the test. Generally, 5 to 15 fibers were tested to estimate the mean interfacial shear strength. The thermal fatigue resistance of composite specimens was determined by measuring the interfacial shear strength of thermally cycled specimens after performing 500 thermal cycles in air on samples in the temperature range 400 K (15 minute soak) to 1100 K (10 minute soak). To avoid the stress relief effects associated with cut ends, discs for the pushout test were cut from the central portions of thermally cycled bars.

The debonded fiber-matrix interfaces and the surface integrity of sapphire fibers extracted from the composite specimens were examined using optical microscopy and scanning electron microscopy (SEM). The fibers were extracted from the matrix by chemically dissolving the matrix in a solution of 75 pct acetic acid (glacial), 23 pct nitric acid, and 2 pct hydrochloric acid. The chemical compositions of fabricated specimens were determined using the inductively coupled plasma (ICP) technique, and the oxygen content was determined using the LECO* nitro-

*LECO is a trademark of LECO Corporation, St. Joseph, MI.

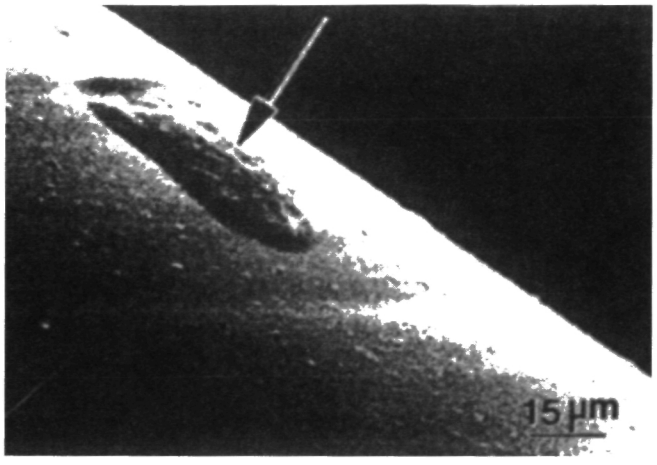

(*a*)

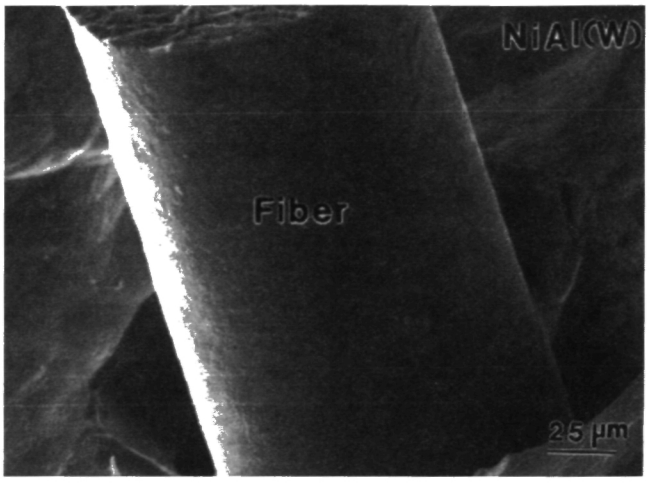

(*b*)

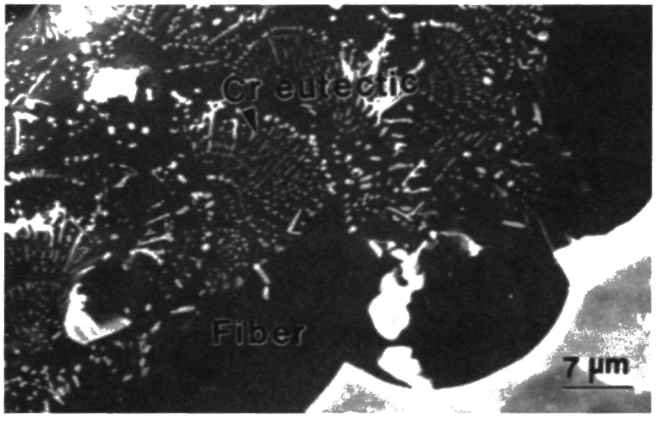

(*c*)

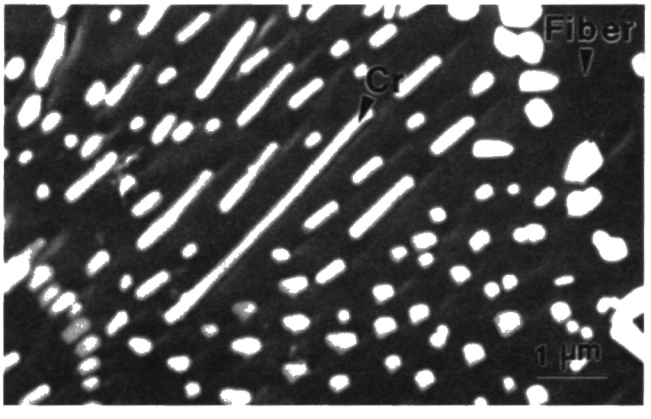

(*d*)

Fig. 2—SEM views of (*a*) as received sapphire fiber, (*b*) sapphire fiber extracted from the DS NiAl(W), (*c*) NiAl-Cr eutectic adhering to the surface of fiber extracted from a DS NiAl(Cr) specimen, and (*d*) higher magnification view of a region of (c) showing fine grooves on fiber surface.

gen/oxygen determinator. The measurements of microhardness on transverse sections as a function of the distance from the fiber-matrix interface were made on NiAl and NiAl(Cr) specimens using a Buehler Microhardness tester, with a knoop indentor and 300 g load.

III. RESULTS

A. *Chemistry and Microstructure*

The compositions (in weight percent) of NiAl(Cr) and NiAl(W) alloys, determined to 5 pct relative accuracy, were 28.2Al-11.4Cr-60.2Ni and 31.4Al-1.5W-67.4Ni, respectively. The average oxygen content to 10 pct relative accuracy was about 300 ppm. Figure 1 shows typical microstructures of as cast (AC) and DS sapphire-NiAl(Cr) specimens and AC and DS sapphire-NiAl(W) specimens. The DS NiAl(Cr) matrix (Figure 1(c)) exhibited a cellular structure, with the eutectic occupying the intercellular regions. Both AC and DS sapphire-NiAl(Cr) specimens showed preferential deposition of NiAl Cr eutectic on the fiber surface (Figures 1(a) and (b)). However, unlike the NiAl(Cr) specimens, the AC and DS NiAl(W) specimens did not show preferential segregation of tungsten rich phases at the fiber-matrix interface. Large columnar grains of NiAl aligned parallel to the growth direction characterized the matrix microstructure of DS specimens, as shown in Figure 1(g). This figure shows two regions, corresponding to two growth speeds, on a longitudinal section. At the lower growth speed of 3 $\mu m \cdot s^{-1}$, a planar solid liquid interface formed and resulted in large columnar grains aligned along the growth direction (region A in Figure 1(g)). At a higher growth speed of about 11 $\mu m \cdot s^{-1}$, the initially planar solid liquid interface broke down into an aligned cellular structure, with the intercellular regions occupied by the eutectic (region B in Figure 1(g)). The DS microstructure shown in Figure 1(f) is from a transverse section of the high growth rate region of type B in Figure 1(g).

Chromium precipitates are present within the NiAl cells (Figure 1(c)) and are formed by the solid-state precipitation of chromium from the supersaturated NiAl matrix, upon cooling at the conclusion of the DS process. The chromium particles in the NiAl-Cr eutectic appear to be well bonded to the fiber (Figure 1(d)), and the two have not separated during the cooldown from the processing temperatures.

The sapphire fibers in the DS NiAl(Cr) alloys are surrounded by two types of microstructures, as indicated by regions C and D in Figure 1(d). If a large region of intercellular NiAl-Cr eutectic solidifies in contact with the fiber,

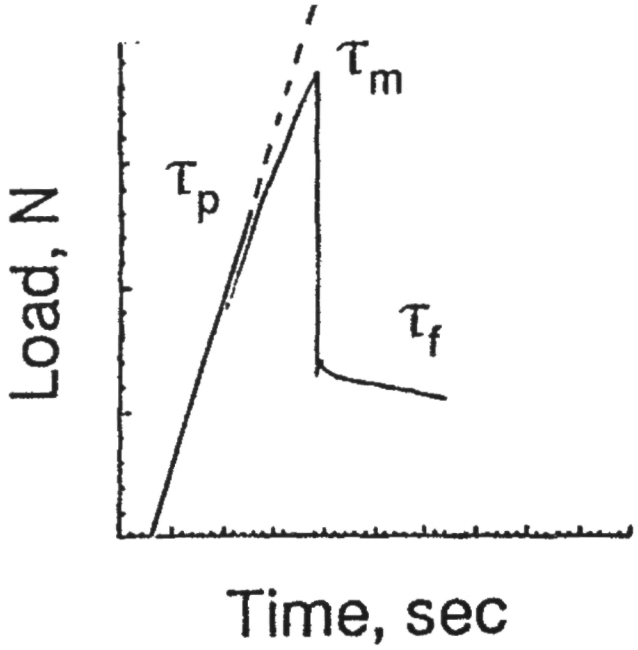

Fig. 3—Schematic load time plot from the fiber pushout test and definition of shear stresses, τ_p, τ_m, and τ_f.

Table I. Interfacial Shear Strengths of Various Sapphire-NiAl Composites

Material	τ_p (MPa)	τ_m (MPa)*	τ_f (MPa)
AC NiAl (Cr)	114 ± 36	154 ± 55	72 ± 39
AC + TC NiAl(Cr)	93 ± 39	> 104 ± 38(2)	43 ± 27
DS NiAl(Cr)	127 ± 47	> 155 ± 41(1)	72 ± 35
DS + TC NiAl(Cr)	146 ± 40	> 174 ± 40(5)	91 ± 41
AC NiAl(W)	158 ± 71	> 168 ± 70(3)	41 ± 24
DS NiAl(W)	100 ± 41	> 159 ± 69(1)	28 ± 13
DS + TC NiAl(W)	—	> 127 ± 68(1)	—
AC NiAl	91 ± 60	133 ± 79	48 ± 40
DS NiAl	78 ± 32	> 182(4)	10
DS + TC NiAl	142 ± 37	> 170 ± 17(3)	—
PC NiAl	30 ± 14	42 ± 21	22 ± 9
PC + DS NiAl	84 ± 40	138 ± 62	27 ± 7
Binderless NiAl[25]	—	> 280	—

*The sign ">" preceding the τ_m values indicates that the loading limit of the instrument was reached before the fiber could be pushed out. The number of fibers that could not be pushed out is shown in parentheses adjacent to the corresponding τ_m values.

the microstructure of region C results, with finely distributed NiAl-Cr eutectic surrounding the fiber. If, on the other hand, the intercellular eutectic melt region in contact with the fibers is relatively small, the β of the solidifying β-Cr eutectic grows on the pre-existing primary β cells. The sapphire fiber, therefore, appears to be surrounded by relatively coarse chromium eutectic particles and β-NiAl (region D in Figure 1(d)).

Figure 2 compares the surface appearance of as received fibers and fibers extracted from the DS specimens. The as received fibers occasionally contained growth related surface flaws, indicated by the arrow in Figure 2(a). No gross fiber damage, other than the original growth related flaws, could be resolved at these magnifications in the NiAl(W) specimens (Figure 2(b)). In the case of sapphire-NiAl(Cr) specimens, fine precipitates of a chromium-rich phase were observed to adhere to the surfaces of extracted fibers (Figures 2(c) and (d)), as confirmed from energy dispersive spectroscopy (EDS) analysis. These precipitates appear to reside in fine pits on the fiber surface, which may have formed from a chemical reaction between sapphire and chromium. Each chromium particle appears to be associated with an identically shaped ridge, with the population density of particles and ridges being roughly equal over the fiber segments examined. That these surface defects actually formed due to fiber-matrix interaction rather than due to a chemical attack of fibers by the etchant used to dissolve the matrix was confirmed through independent SEM examination of virgin fibers that were kept in contact with the etchant for prolonged periods.

B. *Fiber Pushout Behavior*

A schematic load time profile from the fiber pushout test on composites is shown in Figure 3. In all the cases, an initially linear (pseudoelastic) load-displacement response was followed by a nonlinear (inelastic) response, which concluded in a sharp load drop accompanied by large-scale displacement of the fiber. The pushout behavior is characterized in terms of the following parameters:[6] the limiting proportional shear stress, τ_p (transition between linear and nonlinear regions), the maximum shear stress, τ_m (corresponding to final debonding), and the frictional shear stress, τ_f (corresponding to large scale, postdebond fiber displacement). These shear stresses were computed using the relationship $\tau = F/\pi Dt$, where τ is the shear stress, F is the load, D is the fiber diameter, and t is the thickness of the disc. The τ_f values were computed at frictional loads corresponding to an arbitrary displacement of 8 μm beyond the τ_m.

1. *Proportional Shear Stress (τ_p), Maximum Shear Stress (τ_m), and Frictional Shear Stress (τ_f)*

a. *Sapphire NiAl(Cr)*

Table I summarizes the mean values of τ_p, τ_m, and τ_f for different composites tested in the present study. This table shows that the mean value of τ_p of the AC and DS NiAl(Cr) are about 25 to 60 pct higher compared to the τ_p values of the AC and DS NiAl specimens. The PC processed specimens and the PC + DS NiAl specimens have τ_p values lower than both AC and DS NiAl specimens, as well as AC and DS NiAl(Cr) specimens. The TC of AC and DS NiAl(Cr) appears to have little effect on the proportional shear stress. The τ_p values of the AC and DS NiAl(Cr) after thermal cycling are similar to their τ_p values prior to TC. The test specimens in the present study were low fiber volume fraction composites (<0.5 vol pct) with interfiber spacings roughly an order of magnitude larger than the fiber diameter. Therefore, the measured interfacial shear strengths of thermal cycled specimens probably do not represent the true TC resistance of a structurally viable NiAl matrix composite reinforced with larger fiber volume fractions.

The maximum shear stress, τ_m, represents onset of shear instability and catastrophic failure of the interface accompanied by large scale fiber displacements. The numbers in parentheses adjacent to the mean τ_m values in Table I indicate the number of fibers that could not be debonded before reaching the load capacity of the instrument. The

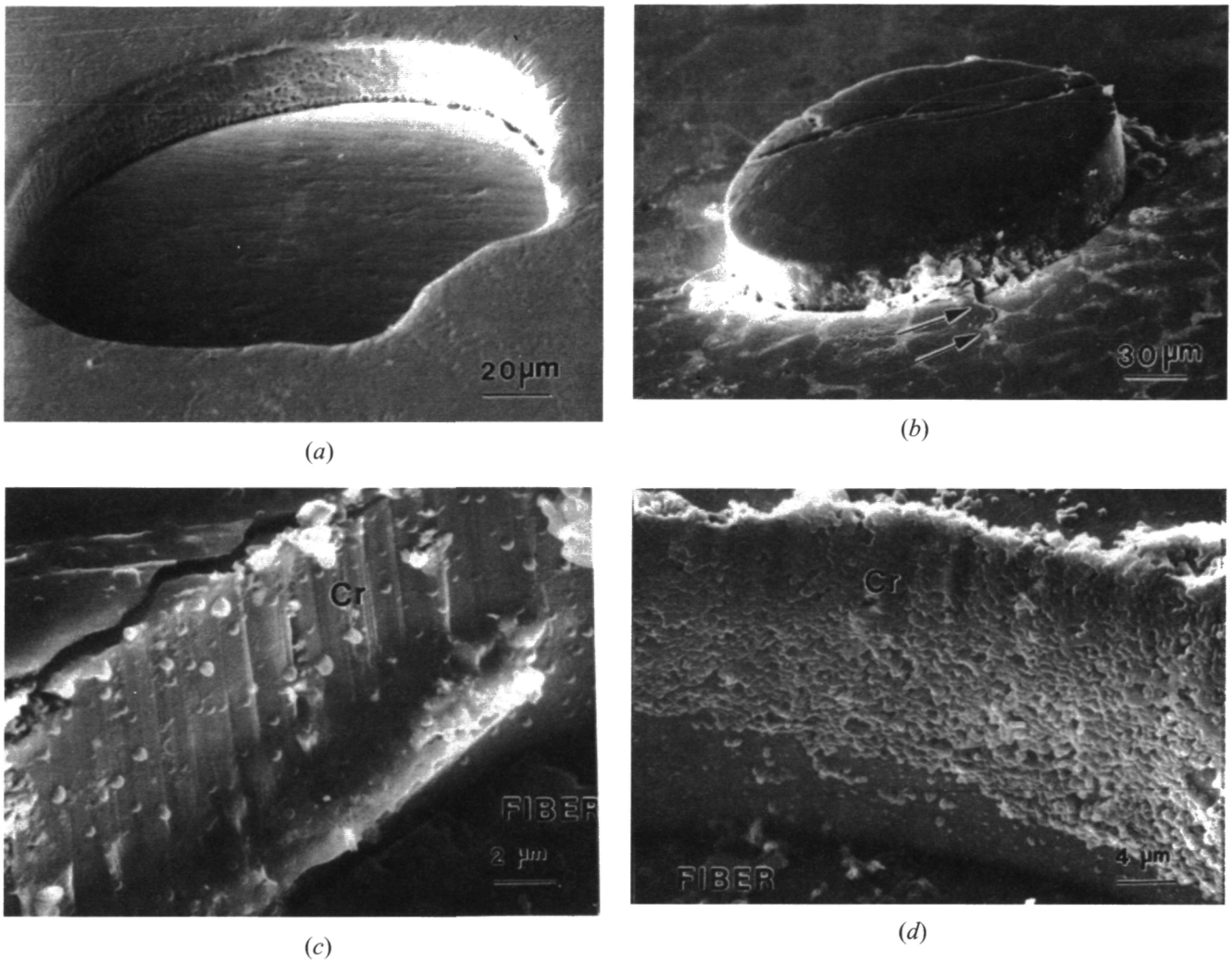

Fig. 4—SEM views of debonded fiber matrix interfaces in sapphire NiAl(Cr) composite during the pushout test: (*a*) front face (facing the punch), (*b*) back face, (*c*) wear tracks caused by Cr precipitates and fiber asperities during postdebond sliding of fiber relative to the matrix, and (*d*) SEM view of the debonded matrix surface in the region of displaced fiber showing NiAl Cr eutectic at the interface.

maximum shear stresses in these composites are reported as being greater than the values shown (hence the use of symbol ">" for τ_m in Table I). Table I shows that chromium addition to NiAl does not impair the maximum shear stress of the sapphire-NiAl bond. Also, no dramatic reduction in the τ_m values is noted as a result of thermal cycling (e.g., the mean τ_m values for the AC NiAl(Cr) specimens decreased by about 30 pct). On the other hand, the τ_m value for the DS NiAl(Cr) increased marginally after TC. While the τ_m of NiAl(Cr) is significantly higher than the τ_m of the PC and PC + DS sapphire NiAl(Cr) composites,[6] the strength of the binderless PC sapphire-NiAl (>280 MPa) is larger than that of cast and DS sapphire-NiAl(Cr).

The mean values of the frictional shear stress, τ_f, for the AC and DS NiAl(Cr) specimens are higher than the τ_f values of the unalloyed specimens made from cast or hot pressed (PC) feedstock. The chromium interlayer surrounding the sapphire fibers in the NiAl(Cr) specimens conceivably led to an increase in τ_f compared to the unalloyed NiAl specimens. Also, since this chromium interlayer is present on the fiber surface regardless of the fabrication technique used, no difference in the τ_f values was observed between AC and DS NiAl(Cr) specimens.

b. *Sapphire-NiAl(W) composites*

Table I shows that cast and DS NiAl(W) specimens have a higher τ_p compared to both cast and DS NiAl as well as PC and PC + DS NiAl. The mean τ_m of AC and DS NiAl(W) is significantly higher than the τ_m of PC NiAl. On the other hand, the τ_m of NiAl(W) is only marginally greater than that of PC + DS NiAl and comparable to the τ_m of AC and DS NiAl. Thermal cycling leads to a reduction (<20 pct) in mean τ_m. The frictional shear stress, τ_f, of AC and DS NiAl(W) is lower than the τ_f of NiAl(Cr) and is comparable in magnitude to the τ_f of unalloyed AC and DS NiAl. Unlike the NiAl(Cr) specimens, where an interlayer of chromium rich eutectic surrounds the sapphire, the fiber-matrix interfaces in the NiAl(W) as well as those in the unalloyed NiAl specimens[5,6] are relatively clean and do not show an excess of any phase(s).

C. *Fracture Behavior of PushOut Specimens*

1. *Sapphire-NiAl(Cr)*

Figure 4 shows front face (facing the punch) and back face SEM views of debonded fiber and matrix surfaces after interrupting the test in the frictional regime. Figures 4(c)

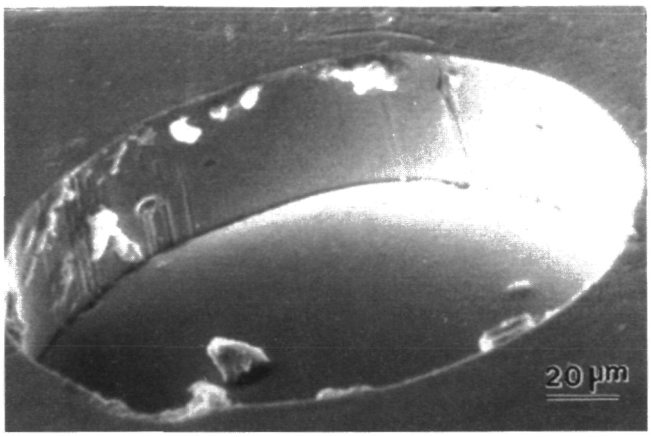

(*a*)

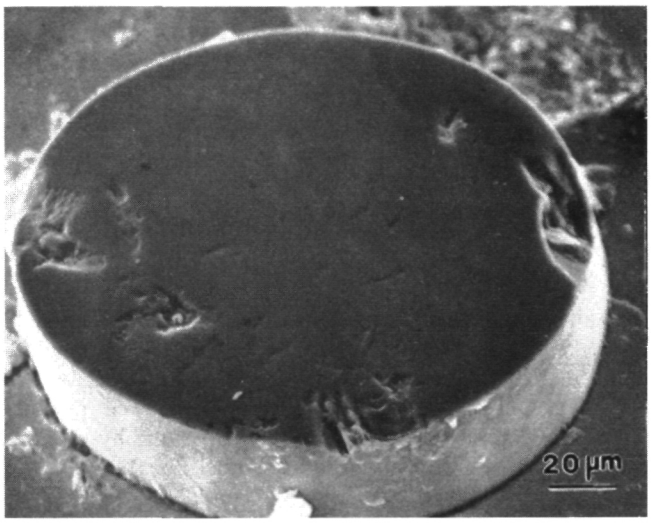

(*b*)

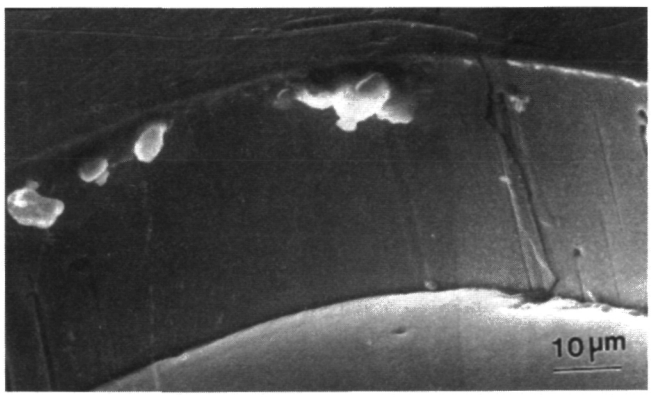

(*c*)

Fig. 5—SEM views of debonded fiber matrix interface in sapphire NiAl(W) composite: (*a*) front face (facing the punch), (*b*) back face, and (*c*) higher magnification view of debonded matrix surface in the region of displaced fiber showing clean interface and some wear marks.

and (d) are higher magnification SEM views of the front faces of two typical pushed out fibers. The front faces of the test specimens with pushed fibers are crack free, whereas the back faces show fine radial cracks (marked by arrows in Figure 4(b)) that follow the intercellular eutectic colonies, which presumably provide an easy path for crack growth. The propagation of these cracks through the intercellular eutectic is analogous to the growth of back face cracks along matrix grain boundaries coincident on the fiber surface in unalloyed sapphire-NiAl.[6] The chromium particles decorate the debonded matrix surface in the region of displaced fiber (Figures 4(c) and (d)).

The interfacial debond shear stress in NiAl(Cr) appears to depend upon a fiber's microstructural surroundings. Thus, for the fiber surrounded by a continuous layer of fine NiAl(Cr) eutectic (region C in Figure 1(d) and the debonded surface in Figure 4(d)), the τ_m and τ_f are 125 and 76 MPa, respectively. On the other hand, for the fiber in contact with the β-NiAl cells and surrounded by the sparsely distributed chromium (region D in Figure 1(d) and the debonded surface in Figure 4(c)) the τ_m and τ_f were 223 and 152 MPa, respectively. This dependence of interfacial shear stresses on the local microstructural surroundings was observed for most of the tested fibers. Note, however, that the total displacement of the fiber during push-out was roughly comparable to the longitudinal cell size in the DS material; over the entire thickness of the test specimen (300 to 400 μm), any given fiber will likely encounter both these types of microstructural regions at different locations over its embedded length. Also, small fluctuations in growth rate or temperature gradient during directional solidification will result in wavy rather than straight cell walls. Therefore, it is perhaps somewhat naive to assign the differences in the debond and frictional shear stresses to the microstructural features observed only at the top or bottom planes of the test specimens, especially because the distribution of chromium will not be uniform over the embedded fiber length. As a result, the modulation of thermoelastic clamping stresses prior to debonding and the contribution of spatial distribution of chromium particles to asperity controlled friction during postdebond sliding cannot be related strictly to the spatial density of chromium at the top and bottom surfaces of test specimens.

The chromium particles, together with the surface asperities in the original fiber, presumably cause microplastic grooving (Figure 4(c)) of the matrix during fiber sliding; similar matrix grooving due to fiber asperities was earlier observed in PC sapphire-NiAl.[16] The width of grooves (about 2 μm) on the debonded matrix surface is about the same as the average size of chromium precipitates adhering to the debonded matrix surface. The debonded interfaces were much cleaner in cast and DS sapphire-NiAl,[5] which also agrees with the relatively lower frictional shear stress of these materials, Table I.

2. *Sapphire-NiAl(W) Composites*

No preferential precipitation of tungsten-rich eutectic was observed on the fiber surface with up to 1.5 pct tungsten additions to NiAl. Consequently, no significant enrichment of second phases is anticipated at the debonded matrix surface from the pushout test. Figure 5 shows the front and back face SEM views of debonded fiber and matrix surfaces in the sapphire NiAl(W) specimens. The debonded surfaces are clean but show some wear tracks, presumably due to the microplastic grooving by fiber asperities (Figure 5(c)). In contrast to NiAl(Cr), the back faces of tested specimens do not show microcracks associated with intercellular eutectic regions.

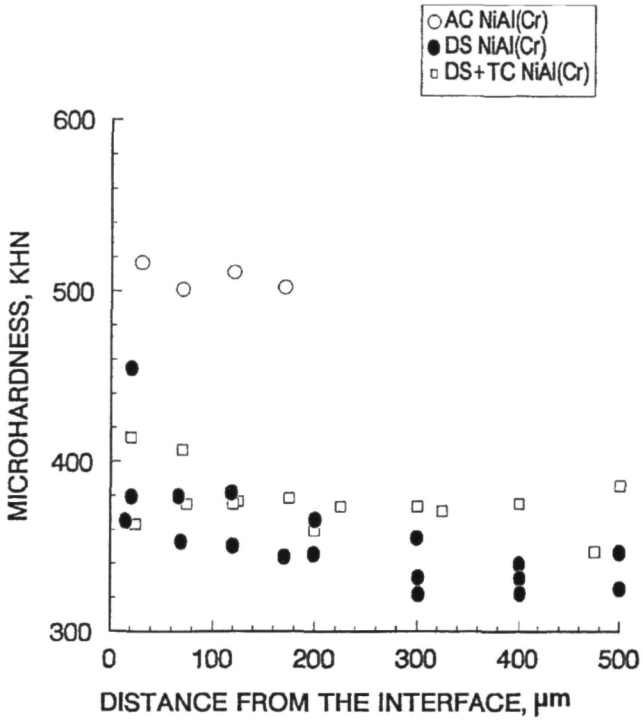

(*a*)

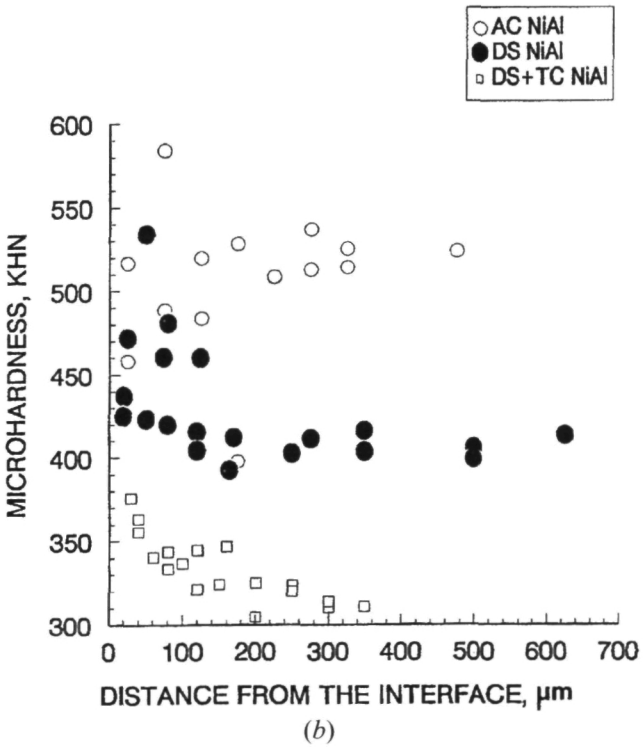

(*b*)

Fig. 6—The variation of matrix microhardness with the distance from the fiber matrix interface in (*a*) sapphire NiAl(Cr) and (*b*) sapphire NiAl specimens.

D. *Microhardness Distribution across the Fiber Matrix Interface*

The variation of matrix microhardness with the distance from the fiber-matrix interface for the NiAl and NiAl(Cr) specimens in the as cast, DS, and TC conditions is shown in Figure 6(a). The microhardness at any given location of cast NiAl and NiAl(Cr) shows considerable scatter and no systematic variation with the distance from the fiber surface; the average hardness of 501 KHN for the NiAl(Cr) is comparable to the average hardness of 513 KHN for the NiAl. The DS specimens, on the other hand, show a gradient of hardness with the highest hardness occurring near the fiber surface. The distance (about 175 μm) at which the hardness gradient becomes roughly zero in the DS NiAl and DS NiAl(Cr) is approximately equal to one fiber diameter. The average hardness in the matrix away from the interface is higher in the DS NiAl (400 KHN) than in the DS NiAl(Cr) (333 KHN).

Thermal cycling significantly reduces the hardness gradient near the interface in the DS NiAl(Cr). However, the microhardness gradient near the interface, within a distance equal to about one fiber diameter, is still present in the DS + TC NiAl specimens. Thermal cycling appears to reduce the hardness of DS NiAl (from 400 to 300 KHN) but does not seem to affect the hardness of DS NiAl(Cr) specimens. In fact, a slight increase of microhardness is noted after thermal cycling, from 333 to 360 KHN, for the DS NiAl(Cr).

IV. DISCUSSION

A. *Wetting and Interface Strength*

While the wetting and bond strength data on sapphire-NiAl are scarce, it has been reported that the wetting angle and "pushoff" bond strength of sapphire and nickel are 112 deg and 82.1 MPa, respectively.[10,11] The pushoff strengths in these investigations were measured by pushing the solidified sessile drops (furnace cooled) off the sapphire substrate by application of a stress parallel to the sapphire plaque at the base of the droplet. These studies showed that the addition of Cr to Ni at Cr contents greater than approximately 1 wt pct decreased the wetting angle of Ni on sapphire, and at 10 wt pct Cr in Ni, the wetting angle and pushoff bond strength values were 90 deg and 108 MPa,[10] respectively. The value of 108 MPa for strength compares favorably with the fiber pushout strength (125 MPa) of sapphire-NiAl(Cr) specimens in the present study, when the fiber was located within a eutectic colony (Figure 4(d)). Since the cooling of Ni-Cr droplets in Reference 10 must have commenced at the top surface of the droplet (the furnace was switched off in order to cool and solidify the droplet), solidification must have progressed toward the sapphire substrate rather than starting from it. Under these conditions, the last freezing eutectic liquid (the Ni-Cr system forms a eutectic at 1345°C and 51 wt pct Cr) will solidify preferentially on the sapphire substrate that supported the droplet, a situation microstructurally analogous to the case of a sapphire fiber embedded in a eutectic colony (Figure 4(d)). The agreement between the estimates of interface strengths from the two studies is, then, quite encouraging despite differences in the matrix chemistries.

The fiber-matrix interfacial shear strength is determined by three factors: (a) the thermal clamping stresses due to coefficient of thermal expansion (CTE) mismatch between the fiber and the matrix, (b) chemical bonding between the fiber and the matrix, and (c) the mechanical interlocking with the matrix of surface asperities and diametric assymetries of the fiber (frictional bonding). The CTE mismatch

between NiAl and sapphire [$\alpha_{sapphire} = 9.5 \times 10^{-6}$ K^{-1}[3] and $\alpha_{NiAl} = 15 \times 10^{-6}$ K^{-1}[3]] is large and results in thermal clamping stresses that are compressive in the fiber and tensile in the surrounding matrix.[15,16,17] Thus, as a result of combined loading from the applied mechanical stress and the thermal clamping stresses, the overall interfacial stress state in the "thin slice" pushout test is greatly modified.[16,17] The large, compressive radial stresses created by the thermal stresses over most of the fiber length tend to increase the magnitude of pushout stress. The thermal clamping stresses due to CTE mismatch between the fiber and the matrix are expected to be lower in the NiAl(Cr) than in NiAl, since chromium, which forms an interlayer on the fiber surface, has a lower CTE ($\alpha_{Cr} = 6.2 \times 10^{-6}$ K^{-1}[18]), and therefore has a better match with the CTE of sapphire as compared to NiAl. If the thermal clamping stresses were the dominant contributor to the measured interfacial shear strength, the cast and DS sapphire-NiAl(Cr) would have yielded a lower interfacial shear strength as compared to cast and DS sapphire NiAl. The fact that the observed behavior (Table I) is in fact opposite to this is probably due to chemical modification of the fiber-matrix interface by chromium alloying.

While it will be necessary to assess the high temperature stability of NiAl-Cr eutectic interlayers on fiber surface before these materials can be recommended as potential candidates for high temperature strengthening, the preliminary thermal cycling test results were quite encouraging and showed that thermal cycling in air in the temperature range 400 to 1100 K did not appreciably degrade the interfacial shear strength of sapphire-NiAl(Cr) (Table I). This seems to suggest that the compliant layer of chromium at the fiber matrix interface does not lose its effectiveness as a result of limited thermal cycling of composites carried out in air under the testing conditions of the present study.

B. *Interfacial Reactions*

Evidence of chemical attack of sapphire by chromium of the matrix was noticed from the microscopic examination of extracted fibers (Figure 2). The resulting surface ridges and pits on fiber could serve to concentrate stress and cause premature fiber failure. The critical size, c, at which a surface flaw extends into a damaged fiber is related to the fiber tensile strength, σ_f, by[19] $\sigma_f = 0.893\ (E_f G_c/\pi c)^{0.5}$, where E_f is the fiber modulus, and G_c $(=K_{Ic}^2 c/E_f)$ is the strain energy release rate of fiber. For single crystal alumina, $K_{Ic} = 2.38$ MPa·$m^{0.5}$,[20] $E_f = 435$ GPa,[21] and $\sigma_f = 2.7$ GPa,[21] so that flaw size c is obtained as 0.2 μm. While the surface flaws on extracted sapphire fibers (Figure 2(d)) appear to be somewhat smaller than 0.2 μm, it is difficult to prove conclusively that these flaws will not be strength-limiting. Past work[20,22,23] has shown that the strength of single crystal sapphire fiber (SAPHIKON) degrades by almost 50 pct in solid state processed composites based on NiAl and other intermetallic and superalloy matrices. Clearly, the issue of fiber strength loss due to chemical reactions in the NiAl(Cr) matrices cannot be satisfactorily resolved at this time.

C. *Microhardness*

The CTE mismatch induced stresses contribute to the buildup of microhardness in the vicinity of the fiber. The

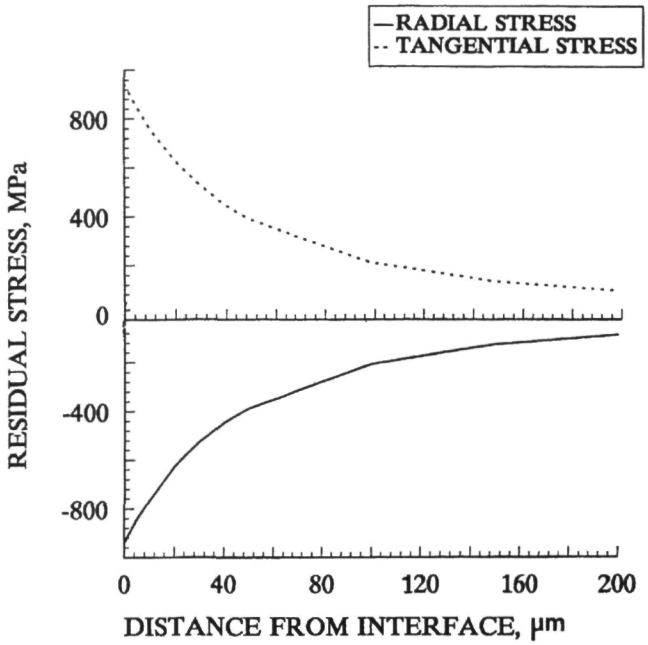

Fig. 7—Theoretical variation of radial and tangential stresses due to CTE mismatch between the sapphire fiber and the NiAl matrix as a function of the distance from the fiber-matrix interface.

stress distribution can be computed as a function of the distance from the fiber-matrix interface using a CTE mismatch based interfacial stress model,[24] which assumes that both fiber and matrix are under elastic strain. In this model, a cylindrical fiber matrix geometry is analyzed considering the CTE mismatch, $\Delta\alpha$, fiber volume fraction, V_f, fiber diameter, $2a$, elastic modulii of matrix and fiber materials (E_f and E_m), and poisson's ratio of the fiber and the matrix materials. Analytical expressions from the model for the radial stress (σ_{rr}) and tangential stress ($\sigma_{\theta\theta}$) distributions were used to compute the variation of these stresses as a function of the distance from the fiber-matrix interface.

For the sapphire-NiAl specimens used in the present study, $2a = 180$ μm, $\Delta\alpha = 5.5 \times 10^{-6}$ K^{-1}, $\upsilon_m = \upsilon_f = 0.3$, $E_m = 230$ GPa, $E_f = 435$ GPa, $V_r = 0.22$ pct, and $\Delta T = 1600$ K. Figure 7 shows a plot of radial and tangential stress distributions in the matrix as functions of the distance from the fiber-matrix interface. The tangential stress ($\sigma_{\theta\theta}$) is tensile (positive) and radial stress (σ_{rr}) is compressive (negative). Near the fiber surface, both the radial and tangential stresses are very large (about 1000 MPa), and they decrease systematically to zero at distances greater than about 180 to 200 μm. The influence of thermal stresses appears to be confined to distances on the order of one fiber diameter. For distances smaller than about 100 μm, the radial and tangential stresses are large and may exceed the yield strength of the matrix (about 380 MPa for NiAl[17]). Since no interfacial cracks were observed in the DS specimens, these stresses must have been accommodated by localized plastic deformation of the matrix.

A hardness gradient is observed in the vicinity of the fiber in the DS NiAl and DS NiAl(Cr), whereas the hardness gradient is eliminated in the cast specimens. In the cast specimens, the high quenching rates in the copper mold prevent stress relief in the bulk matrix, thereby yielding increased matrix microhardness. On the other hand, the rel-

atively slow cooling rates during directional solidification permit thermal stresses in the matrix to be partially relieved; as a result, the average matrix microhardness in the DS material is lower than that in the as cast material. The residual stresses arising from the CTE mismatch will be confined to matrix regions in the immediate vicinity of the fiber. In the as cast specimens, the large quenching stresses presumably over ride the CTE induced stresses; as a result, no gradient of hardness is observed. On the other hand, the relatively slow cooling rates of the DS specimens permit some stress relaxation so that stresses arising from the CTE mismatch are displayed in the hardness trace as a gradient near the fiber surface.

Since the composite specimens used in the present work had near-zero (<0.5 pct) volume fraction of the fiber, there is virtually no overlap between neighboring fibers of stress profiles due to CTE mismatch. As a result, a distinct gradient of microhardness trace is observed in slow cooled DS specimens. However, this behavior may not be observed in a real composite with appreciably larger fiber volume fractions.

V. CONCLUSIONS

1. This investigation has shown that chromium and tungsten alloying of NiAl improves the strength of the sapphire-NiAl interfacial bond without causing appreciable additional fiber damage. The proportional shear stress, τ_p, the maximum shear stress, τ_m, and the frictional shear stress, τ_f, obtained by a fiber pushout test, for the AC and DS sapphire-NiAl(Cr) and sapphire-NiAl(W), are higher than those of AC and DS sapphire-NiAl.
2. In the case of sapphire-NiAl(Cr), a compliant layer of chromium-rich eutectic forms at the fiber-matrix interface. On the other hand, no interfacial excess of tungsten-rich phases is observed in the sapphire-NiAl(W) specimens. The higher interfacial bond strength of sapphire-NiAl(Cr) is likely a result of chemical modification of the interface by chromium.
3. The improvement in the interfacial shear strength of DS NiAl(Cr) and NiAl(W) over DS NiAl suggests that dual-phase microstructures (β-NiAl surrounded by eutectic), having improved room-temperature ductility and toughness, can be produced by directional solidification of NiAl alloys. These DS alloys can be further reinforced with sapphire fibers to achieve improvements in both the room-temperature toughness and the high-temperature strength.

ACKNOWLEDGMENTS

Appreciation is expressed to Thomas K. Glasgow, Chief, Processing Science and Technology Branch, NASA Lewis Research Center, for provision of experimental facilities; J.I. Eldridge, Surface Science Branch, for helpful discussion on the fiber pushout test; and R.R. Bowman, Intermetallics Branch, for a critical review of the manuscript. One of the authors (RA) acknowledges the award of an associateship by the National Research Council, Washington, DC.

REFERENCES

1. Darolia: *J. Met.*, 1991, vol. 43 (3), p. 44.
2. R.D. Noebe, A. Misra, and R. Gibala: *J. Iron Steel Inst. Jpn.*, 1991, 31, 1172–1186.
3. R.D. Noebe, R.R. Bowman, and J.I. Eldridge: *Intermetallic Matrix Composites*, Materials Research Society Symposia Proceedings, D.L. Anton, R. McMeeking, D. Miracle, and P. Martin, eds., p. Materials Research Society, Pittsburgh, PA, vol. 194, p. 323–331.
4. J.W. Pickens, R.D. Noebe, G.K. Watson, P.K. Brindley, and S.L. Draper: *NASA TM 102060*, 1989.
5. S.N. Tewari, R. Asthana, and R.D. Noebe: *Metall. Trans. A*, 1993, vol. 24A, pp. 2119–25.
6. R. Asthana, S.N. Tewari, and R.R. Bowman: *Metall. Mater. Trans. A*, 1995, vol. 26A, p. 209–223.
7. D. Xu, D. Wang, and T.L. Lin: *Scripta Metall.*, 1993, vol. 26, p. 599.
8. S.L. Draper, D.J. Gaydosh, and M.V. Nathal: *J. Mater. Res.*, 1990, vol. 5, p. 1976.
9. S. Nourbakhsh, O. Sahin, W.H. Rhee, and H. Margolin: *Metall. Trans. A*, 1991, vol. 22A, pp. 3059–64.
10. R.M. Crispin and M. Nicholas: *J. Mater. Sci.*, 1976, vol. 11, p. 17.
11. M. Nicholas: *J. Mater. Sci.*, 1968, vol. 3, p. 571.
12. S.N. Tewari: NASA TN D 8355, 1977.
13. D.R. Johnson, S.M. Joslin, B.F. Oliver, R.D. Noebe, and J.D. Whittenberger: *Intermetallic Matrix Composites II*, Materials Research Society Symposia Proceedings, D.B. Miracle, J. Graves, and D. Anton, eds, Materials Research Society, Pittsburgh, PA, 1992, vol. 273, p. 87–92.
14. J.I. Eldridge: NASA TM 105341, 1991.
15. A.K. Misra: NASA CR 191167, 1993.
16. D.A. Koss, M.N. Kallas, and J.R. Hellman: *Intermetallic Matrix Composites II*, Materials Research Society Symposia Proceedings, D.B. Miracle, J. Graves, and D. Anton, eds, Material Research Society, Pittsburgh, PA, 1992, vol. 273, p. 303.
17. M.N. Kallas, D.A. Koss, H.T. Hahn, and J.R. Hellman: *J. Mater. Sci.*, 1992, vol. 27 (4), p. 3821.
18. *Metals Handbook*, 8th ed., ASM, Metals Park, OH, 1961, vol. 1, p. 48.
19. S. Ochiai and K. Osamura: *Metall. Trans. A*, 1988, vol. 19A, pp. 1499 1506.
20. S.L. Draper and I.E. Locci: *J. Mater. Res.*, 1994, vol. 9 (6), p. 1397–1411.
21. "Sapphire and Advanced Single Crystal Technologies" (Data Sheet), Saphikon Inc., Milford, NH.
22. R.R. Bowman, I.E. Locci, S.L. Draper, and A.K. Misra: *Materials Research Society Symposia Proceedings*, Materials Research Society, Pittsburgh, PA, 1994, vol. 350, p. 105–110.
23. R.R. Bowman, A.K. Misra, and I.E. Locci: *NASA HITEMP Proc.*, NASA CP 19117, 1993, vol. II, p. 57–1.
24. A.B. Gokhale, L. Lu, and R. Abbaschian: in *Solidification of Metal Matrix Composites*, P. Rohatgi, ed., TMS, Warrendale, PA, 1990.
25. R.R. Bowman: *Intermetallic Matrix Composites II*, Materials Research Society Symposia Proceedings, D.B. Miracle, J. Graves, and D. Anton, eds., Materials Research Society, Pittsburgh, PA, 1992, vol. 273, p. 145.